Comparing scattering rates from Boltzmann and dynamical mean-field theory

M. Wais,[1,*] J. Kaufmann,[1,*] M. Battiato,[2] and K. Held[1]
[1]*Institute of Solid State Physics, TU Wien, Vienna, Austria*
[2]*Nanyang Technological University, 21 Nanyang Link, Singapore*

(Received 21 December 2020; revised 19 March 2021; accepted 10 May 2021; published 21 May 2021)

We compute scattering rates for electrons in the two-dimensional Hubbard model for a one-orbital metal and Mott insulator and a two-orbital band insulator by means of dynamical mean-field theory (DMFT) and the Boltzmann scattering equation (BSE), which for the considered equilibrium scattering rates is equivalent to second order perturbation theory. As an intermediate method between both, we also consider the BSE without momentum conservation. In the weak interaction regime and for the band insulator, the last two agree to very good accuracy. The BSE with momentum conservation, on the other hand, shows slightly larger scattering rates, and a momentum differentiation of these on the Fermi surface. For the Mott insulator at strong interaction, the DMFT electron scattering rates are much larger and defy a BSE description. Noteworthy, the scattering rates for the band insulator are exceedingly small because—in contrast to the Mott insulator—impact ionization is not mediated by strong (density-density) Coulomb matrix elements.

DOI: 10.1103/PhysRevB.103.205141

I. INTRODUCTION

The electronic structure, i.e., the electronic states and their broadening or scattering rate, is arguably the most fundamental property of a solid. Scattering processes not only affect equilibrium properties but are also essential if a material is driven away from equilibrium. Experimentally, the one-particle scattering rate for the (occupied) electronic states can be measured by angular-resolved photoemission spectroscopy (ARPES) [1,2]. If vertex corrections can be neglected, there is a one-to-one correspondence between this one-particle scattering rate and the two-particle scattering rates for response functions such as the optical conductivity. Here the width of the Drude peak corresponds to the two-particle scattering rate that, without vertex corrections, is directly related to the one-particle scattering rates we calculate here [3–5]. We study them by using two methods that are widely employed in solid state theory, albeit by different communities. Through our comparison we hope to contribute to a better mutual understanding of the strengths and weaknesses of these methods, as well as of the very different electron-electron scattering in a metal, band insulator, and Mott insulator.

Dynamical mean-field theory (DMFT) [6–9] is one of the most widely used approaches for strongly correlated materials. It is nonperturbative and maps a correlated lattice model onto the solution of an Anderson impurity model in a self-consistent way [7]. DMFT becomes exact in the limit of high dimensions or a high connectivity of the lattice [6], which implies that the self-energy and hence the scattering rate is momentum independent.

The Boltzmann scattering equation (BSE) [10–13] has been originally developed for gases [10] but is nowadays used to address a multitude of different problems, all the way from nuclear physics to cosmology. Often the transport part of this equation is combined with a crude approximation for the scattering, the relaxation time approximation, to study transport properties. However, the full Boltzmann scattering term can also be included, allowing, e.g., for a highly detailed reconstruction of the thermalization process. Among the possible applications of the full Boltzmann scattering term is the possibility of calculating scattering rates for the equilibrium state. In this case, subsequent scattering events are not considered, and the BSE scattering rate is equivalent to second order perturbation theory (second order PT). These BSE or second order PT scattering rates can be directly compared to DMFT.

To the best of our knowledge such a comparison for various physical situations has not been done in a systematic way and for various physical situations. We attempt to fill this blank spot through this work. Specifically, we study the equilibrium scattering rates for the single-orbital Hubbard model in two dimensions as well as those for a two-orbital band insulator. The BSE is expected to fail at strong interaction U, since it describes the dynamics of the distribution function by a (momentum-resolved) rate equation with the transition rates usually calculated in lowest order perturbation theory in U. DMFT, on the other hand, neglects (as an impurity model is solved) the momentum dependence of scattering (an approximation known to become exact in the limit of high dimensions). A final point is that, while DMFT even allows for the construction of effective (local) scattering matrix elements in form of the two-particle vertex, the Boltzmann scattering term needs them as input and only performs the joint density of states (DOS) integration and, eventually, the time propagation.

In this paper we show that indeed at strong interaction U, i.e., in the Mott insulating phase [14], a BSE or second order

[*]These authors contributed equally to this work.

PT description of the scattering rate is not possible. This is maybe not surprising considering the strong interaction, but it is at odds with the good BSE description [15] of the spectral redistribution caused by impact ionization [16]. The DMFT scattering rate is much higher than what can be expected or understood in a rigid band picture; it is intimately connected with the formation of the Hubbard bands and shoulders therein. Conversely, at weak U we obtain a discrepancy as well. These discrepancies, noticeably larger scattering rates, and a momentum differentiation on the Fermi surface, can be traced back to the momentum conservation or lack thereof: DMFT and BSE without momentum conservation are in good agreement.

This paper is structured as follows: In Sec. II we introduce the Hubbard-type models considered, and describe how scattering rates are calculated in DMFT and with the Boltzmann scattering equation. In Sec. III we present results for the weak-coupling single-orbital Hubbard model. Next, we compare scattering rates for the two-orbital band insulator in Sec. IV and the Mott insulating single-orbital Hubbard model in Sec. V. In Sec. VI we discuss the aspects of larger DMFT scattering rates in the Mott insulator and the difference of impact ionization in a band insulator and Mott insulator. In Sec. VII we summarize the results. Furthermore, we provide additional derivations and results in the Appendices.

II. MODEL AND METHODS

A. Hubbard-type models

In this paper we study the single-orbital Hubbard model on a two-dimensional square lattice, as well as a related two-orbital model which is a band insulator. It is useful to employ second quantization, where operators $c^{(\dagger)}_{\mathbf{k}m\sigma}$ annihilate (create) electrons at momentum $\mathbf{k}$ and spin σ in orbital m. Their Fourier-transformed operators $c^{(\dagger)}_{im\sigma}$ do the same for a lattice site i instead of momentum $\mathbf{k}$; the products $n_{\mathbf{k}m\sigma} = c^{\dagger}_{\mathbf{k}m\sigma} c_{\mathbf{k}m\sigma}$ and $n_{im\sigma} = c^{\dagger}_{im\sigma} c_{im\sigma}$ are the particle number operators for momentum and site occupations, respectively. Both Hubbard-type models can be described by the following Hamiltonian:

$$H = \sum_{\mathbf{k}m\sigma} \epsilon_m(\mathbf{k}) n_{\mathbf{k}m\sigma} + \frac{U}{2} \sum_i \sum_{(l\sigma)\neq(m\sigma')} n_{il\sigma} n_{im\sigma'}. \quad (1)$$

The first term constitutes a tight-binding description of the system. It describes the kinetic energy ("hopping") of noninteracting electrons with crystal momentum $\mathbf{k}$ and a dispersion relation $\epsilon_m(\mathbf{k})$ that is assumed to be diagonal in the orbital index m. This term is diagonal in momentum space.

The second term models the Coulomb repulsion U between electrons. It is strictly local at each lattice site i and, for the sake of simplicity, we take the interaction to be the same within one orbital and between different orbitals. Consistently, there is no Hund's rule coupling, i.e., $J = 0$. A self-interaction is excluded in the sum. We consider both the prevalent single-orbital Hubbard model, where orbital indices m and l are restricted to this single orbital, and a two-orbital band insulator with interaction U. In the latter case, the band gap is encoded in the dependence of $\epsilon_m(\mathbf{k})$ on $m \in \{1, 2\}$ as detailed below.

Due to the exponential scaling of the Fock space needed to represent an N-particle wave function, it is completely impossible to compute the dynamics of every single electron in the system. Instead one is bound to make approximations such as the DMFT, BSE or second order PT, for extracting relevant information from statistically averaged quantities such as distributions or correlation functions.

B. Dynamical mean-field theory

Many-body quantum field theory, which also is the pillar upon which DMFT is built, has the Green's function as its basic one-particle quantity. The retarded Green's function is defined as follows (with operators in the Heisenberg representation) [17]:

$$G_R(\mathbf{k}, m, t) = -i\Theta(t)\langle c_{\mathbf{k}m\sigma}(t) c^{\dagger}_{\mathbf{k}m\sigma}(0) + c^{\dagger}_{\mathbf{k}m\sigma}(0) c_{\mathbf{k}m\sigma}(t)\rangle, \quad (2)$$

$$G_R(\mathbf{k}, m, \omega) = \int_{-\infty}^{\infty} dt\, e^{i\omega t}\, G_R(\mathbf{k}, m, t). \quad (3)$$

Here $\Theta(t) = 0$ for $t < 0$ and 1 for $t > 0$ is the step function; and $\langle \cdots \rangle$ the grand canonical expectation value. One can further define a self-energy

$$\Sigma_R(\mathbf{k}, m, \omega) = \left[G^{(0)}_R(\mathbf{k}, m, \omega)\right]^{-1} - \left[G_R(\mathbf{k}, m, \omega)\right]^{-1} \quad (4)$$

as the difference between (inverse) noninteracting ($U = 0$) Green's function $G^{(0)}_R(\mathbf{k}, m, \omega)$ and interacting (U) Green's function $G_R(\mathbf{k}, m, \omega)$, which contains all effects of the interaction [17]. Here, and similarly in

$$G^{(0)}_R(\mathbf{k}, m, \omega) = \lim_{\alpha \to 0^+} [\omega + \mu + i\alpha - \epsilon_m(\mathbf{k})]^{-1}, \quad (5)$$

the orbital-diagonal dispersion relation allows us to avoid matrix inversions in the orbital indices; μ is the chemical potential.

In DMFT, which becomes exact in the limit of infinite dimensions [6], the momentum dependence of the self-energy is neglected: $\Sigma_R(\mathbf{k}, m, \omega) \to \Sigma_R(m, \omega)$. Thus the one-particle Green's function of the Hubbard model in the DMFT approximation is

$$G_R(\mathbf{k}, m, \omega) = [\omega + \mu - \epsilon_m(\mathbf{k}) - \Sigma_R(m, \omega)]^{-1}, \quad (6)$$

where the $i\alpha$ of Eq. (5) becomes obsolete since $\mathrm{Im}\Sigma_R(\omega)$ is negative. For the actual calculation of this self-energy in DMFT, done through a self-consistent solution of an Anderson impurity model, we refer the reader to Refs. [7,9,18].

Let us instead turn to our actual task, i.e., calculating scattering rates or quasiparticle lifetimes. For the following considerations we drop the orbital (m) dependence, as the Green's function and self-energy are anyhow diagonal in m due to the assumed dispersion relation. If we linearize the real part of the self-energy and parametrize it through the quasiparticle weight Z, i.e., $\mathrm{Re}\Sigma_R(\omega) \approx \mathrm{Re}\Sigma_R(0) + [1 - Z^{-1}]\omega$, we can approximate Eq. (6) as

$$G_R(\mathbf{k}, \omega) \approx Z[\omega - \tilde{\epsilon}(\mathbf{k}) - Z\mathrm{Im}\Sigma_R(\omega)]^{-1}, \quad (7)$$

where the Green's function has a quasiparticle pole at $\omega = \tilde{\epsilon}(\mathbf{k}) = Z[\epsilon(\mathbf{k}) + \mathrm{Re}\Sigma_R(0) - \mu]$, with a Lorentzian broadening of full-width half-maximum of $-2Z\mathrm{Im}\Sigma_R[\tilde{\epsilon}(\mathbf{k})]$. That is,

$\tilde{\epsilon}(\mathbf{k})$ is the quasiparticle energy and the broadening indicates that

$$\frac{1}{\tau[\omega=\tilde{\epsilon}(\mathbf{k})]} = -2Z\mathrm{Im}\Sigma_R[\omega=\tilde{\epsilon}(\mathbf{k})] \tag{8}$$

is the inverse lifetime, also known as scattering rate.

Even more transparent is the role of the lifetime τ when we recapitulate the physical meaning of the time-dependent retarded Green's function Eq. (2). For the special case of zero temperature the system is in the ground state $|\mathrm{GS}\rangle$ and if the momentum $\mathbf{k}$ is not occupied in the ground state, Eq. (2) is reduced to

$$G_R(\mathbf{k},t) = -i\langle \mathrm{GS}|c_{\mathbf{k}}(t)c^\dagger_{\mathbf{k}}(0)|\mathrm{GS}\rangle. \tag{9}$$

That is, at time $t=0$ a particle is added to the system which is thus in the state $|\phi\rangle = c^\dagger_{\mathbf{k}}(0)|\mathrm{GS}\rangle$. Projecting this state onto its propagated version at time $t>0\langle\phi(t)| = e^{iE_{\mathrm{GS}}t}\langle \mathrm{GS}|c_{\mathbf{k}}(t)$ yields the probability amplitude (E_{GS} is the ground state energy) that this state still exists after a time t has elapsed [19]. This motivates the interpretation of $|G_R(\mathbf{k},t)|^2$ as the probability that a state created by addition of a particle at $t=0$ still exists at later time $t>0$. Note that, in contrast, the frequency dependent Green's or spectral function $A(\omega) = -1/\pi\ \mathrm{Im}\mathrm{G_R}(\mathbf{k},\omega)$ already describes the probability density at a given energy ω (without taking the absolute value squared).

In Appendix A we show that this probability is approximately

$$|G_R(\mathbf{k},t)|^2 \propto e^{2Z\mathrm{Im}\Sigma_R[\tilde{\epsilon}(\mathbf{k})]t} \equiv e^{-t/\tau[\tilde{\epsilon}(\mathbf{k})]}, \tag{10}$$

which again leads to Eq. (8) for the lifetime τ.

Technically we calculate the DMFT self-energy on Matsubara frequencies [20] by continuous-time quantum Monte Carlo [21] with symmetric improved estimators [22] using the w2dynamics program package [23,24]. The retarded self-energy at real (physical) frequencies is then obtained by the maximum entropy analytic continuation [25,26] using the program package ana_cont [27]. Note that owing to the symmetric improved estimators, the Monte Carlo noise of the self-energy has a very small amplitude even at high Matsubara frequencies. This improves the quality of the directly analytically continued self-energy also at higher real frequencies.

C. Boltzmann scattering equation

The key quantity of the BSE [10–13] is the distribution function, whose dynamics is described through the leading-order contributions of the particle-particle interaction (for the models considered). In cases where elementary particles interact strongly, it is recommendable to rewrite the Hamiltonian in terms of weakly interacting quasiparticles so that the leading order perturbation theory can be applied to the weaker effective quasiparticle interaction.

Here we assume that a quasielectron description is possible and that these quasiparticles are characterized by a certain set of quantum numbers, namely the momentum $\mathbf{k}$, spin σ, or orbital-index n, and a corresponding quasiparticle dispersion relation $\tilde{\epsilon}_{n\sigma}(\mathbf{k})$. Then the distribution function $f_{n\sigma}(t,\mathbf{k})$ corresponds to the expectation value of the occupation number operator of a single-particle state $n_{\mathbf{k}n\sigma}$ at time t. In the following the spin will be absorbed into the band index for brevity.

The BSE in case of a spatially homogeneous system without external fields but with a fermionic particle-particle scattering reads [11–13]

$$\begin{aligned}\frac{df_{n_0}(\mathbf{k}_0)}{dt} = \frac{1}{2}\sum_{n_1n_2n_3}\int d^dk_1d^dk_2d^dk_3\big[&W_{n_0\cdots n_3}(\mathbf{k}_0\cdots\mathbf{k}_3)\\ &\times\big(\big[1-f_{n_0}(\mathbf{k}_0)\big]\big[1-f_{n_1}(\mathbf{k}_1)\big]f_{n_2}(\mathbf{k}_2)f_{n_3}(\mathbf{k}_3)\\ &-f_{n_0}(\mathbf{k}_0)f_{n_1}(\mathbf{k}_1)\big[1-f_{n_2}(\mathbf{k}_2)\big]\big[1-f_{n_3}(\mathbf{k}_3)\big]\big)\big]\end{aligned} \tag{11}$$

for a d-dimensional system. Here $W_{n_0\cdots n_3}(\mathbf{k}_0\cdots\mathbf{k}_3)$ is defined as

$$\begin{aligned}&W_{n_0\ldots n_3}(\mathbf{k}_0\cdots\mathbf{k}_3)\\ &\quad= w_{n_0\cdots n_3}(\mathbf{k}_0\cdots\mathbf{k}_3)\\ &\qquad\times\delta\big[\tilde{\epsilon}_{n_0}(\mathbf{k}_0)+\tilde{\epsilon}_{n_1}(\mathbf{k}_1)-\tilde{\epsilon}_{n_2}(\mathbf{k}_2)-\tilde{\epsilon}_{n_3}(\mathbf{k}_3)\big]\\ &\qquad\times\sum_{\mathbf{G}}\delta(\mathbf{k}_0+\mathbf{k}_1-\mathbf{k}_2-\mathbf{k}_3+\mathbf{G});\end{aligned} \tag{12}$$

and the scattering amplitude $w_{n_0\cdots n_3}(\mathbf{k}_0\cdots\mathbf{k}_3)$ can be calculated by perturbation theory (Fermi's golden rule) and is $\sim U^2$ (explicit formulas follow in the context of the specific models below). The two delta-distributions $\delta(\cdot)$ ensure momentum and energy conservation at the scattering event and the sum $\sum_{\mathbf{G}}$ runs over all reciprocal lattice vectors $\mathbf{G}$.

In thermal equilibrium, the distribution of electrons is given by the Fermi-Dirac distribution $f_{\mathrm{FD}}(\tilde{\epsilon}) = 1/\{1+\exp[\beta(\tilde{\epsilon})]\}$ with the inverse temperature $\beta = 1/T$, and the chemical potential μ already absorbed in $\tilde{\epsilon}$. The Fermi-Dirac distribution is a fixed point of the Boltzmann equation (11) and therefore properly represents an equilibrium system.

The scattering rate $1/\tau_n(\mathbf{k})$ of a test particle that is added in the state $(n,\mathbf{k})$ in thermal equilibrium can be calculated within the Boltzmann framework as (for a derivation, see Ref. [28])

$$\begin{aligned}\frac{1}{\tau_{n_0}(\mathbf{k}_0)} = \frac{1}{2}\sum_{n_1n_2n_3}\int d^dk_1d^dk_2d^dk_3\big[&W_{n_0\cdots n_3}(\mathbf{k}_0\cdots\mathbf{k}_3)\\ &\times\big(\big\{1-f_{\mathrm{FD}}\big[\tilde{\epsilon}_{n_1}(\mathbf{k}_1)\big]\big\}f_{\mathrm{FD}}\big[\tilde{\epsilon}_{n_2}(\mathbf{k}_2)\big]f_{\mathrm{FD}}\big[\tilde{\epsilon}_{n_3}(\mathbf{k}_3)\big]\\ &+f_{\mathrm{FD}}\big[\tilde{\epsilon}_{n_1}(\mathbf{k}_1)\big]\big\{1-f_{\mathrm{FD}}\big[\tilde{\epsilon}_{n_2}(\mathbf{k}_2)\big]\big\}\\ &\times\big\{1-f_{\mathrm{FD}}\big[\tilde{\epsilon}_{n_3}(\mathbf{k}_3)\big]\big\}\big)\big].\end{aligned} \tag{13}$$

The calculation of the scattering rate above is done numerically with the method presented in Ref. [28]. The scattering rate Eq. (13) derived from the Boltzmann scattering theory [28] is equivalent to second order PT as we show in Appendix C explicitly for the case of the BSE without momentum conservation.

Notice that DMFT scattering rates are only energy (and orbital) dependent. In the BSE we can, on the other hand, add a quasiparticle at every momentum $\mathbf{k}$ which then necessarily has the quasiparticle energy $\tilde{\epsilon}_n(\mathbf{k})$. When we later plot the BSE scattering rates as a function of energy, there will be different $1/\tau_n(\mathbf{k})$'s at the same energy $\tilde{\epsilon}$. Note that the many-body lifetime broadening discussed above also allows us to add particles away from $\tilde{\epsilon}_n(\mathbf{k})$ in DMFT, albeit the spectral

density of such states is strongly suppressed if the broadening is weak.

D. BSE without momentum conservation

Prospective differences between the BSE and DMFT may emerge because of (i) strong coupling effects beyond the perturbative treatment of the scattering in the BSE rate equation and (ii) neglecting the momentum dependence in DMFT. The latter not only reflects in the momentum-independent DMFT self-energy but also in disregarding the momentum conservation at scattering events in DMFT. That is, the DMFT self-energy is calculated from Feynman diagrams to all order in U but with the interaction only on an impurity which per construction breaks momentum conservation.

We can apply the same approximation also to Boltzmann scattering. That is, we remove in Eq. (12) the momentum conserving delta-distributions $\sum_{\mathbf{G}} \delta(\mathbf{k}_0 + \mathbf{k}_1 - \mathbf{k}_2 - \mathbf{k}_3) \to \frac{1}{V_{\mathrm{BZ}}}$, where V_{BZ} is the volume of the first Brillouin zone, as was proposed in Ref. [15]. Equation (13) can then be simplified to a purely energy-dependent scattering rate $1/\tau_n(\epsilon)$ that is calculated as [15,28]

$$\begin{aligned}\frac{1}{\tau_{n_0}(\epsilon_0)} = \frac{1}{2}\sum_{n_1 n_2 n_3}\int d\epsilon_1 d\epsilon_2 d\epsilon_3 \big[\tilde{w}_{n_0\cdots n_3}(\epsilon_0\cdots\epsilon_3) \\ \times \delta(\epsilon_0+\epsilon_1-\epsilon_2-\epsilon_3) A_0^{n_1}(\epsilon_1) A_0^{n_2}(\epsilon_2) A_0^{n_3}(\epsilon_3) \\ \times ([1-f_{\mathrm{FD}}(\epsilon_1)] f_{\mathrm{FD}}(\epsilon_2) f_{\mathrm{FD}}(\epsilon_3) \\ + f_{\mathrm{FD}}(\epsilon_1)[1-f_{\mathrm{FD}}(\epsilon_2)][1-f_{\mathrm{FD}}(\epsilon_3)])\big], \end{aligned} \tag{14}$$

where $A_0^n(\epsilon)$ is the normalized DOS of band n and $\tilde{w}_{n_0\cdots n_3}(\epsilon_0\cdots\epsilon_3)$ is the thus modified scattering amplitude that depends on the energies only.

Notice that in Eq. (14) we have explicitly used the fact that the interaction is itself momentum independent (which is the case for the purely local interaction in the Hubbard model) and further disregarded momentum conservation at the scattering vertex.

In the general case Eq. (14) cannot be derived, but it can be constructed as an approximation [29,30]. In the following we will refer to Eq. (14) as Boltzmann without momentum conservation (BSE without **k**).

Note that the structure of Eq. (14) is way simpler than Eq. (13): it can be computed by inverting analytically the energy-conserving delta distribution in Eq. (14) and then using standard numerical integration techniques.

III. ONE-BAND HUBBARD MODEL AT WEAK COUPLING

As a first comparison, we discuss the case of the prototypical one-band Hubbard model in two dimensions at half-filling. Depending on the strength of the local interaction U and the temperature $T = 1/\beta$, such a system is predicted by DMFT to be either metallic or Mott insulating.

For the weak coupling case we may employ Boltzmann theory with the dispersion relation of the noninteracting Hamiltonian, which is

$$\epsilon(\mathbf{k}) = -2t[\cos(k_x) + \cos(k_y)] \tag{15}$$

for $\mathbf{k} = (k_x, k_y) \in [-\pi, \pi) \otimes [-\pi, \pi)$ (lattice constant $a \equiv 1$; unit-cell volume $V_{\mathrm{UC}} = a^2 = 1$) and the corresponding DOS [31]

$$A_0(\omega) = \int_{\mathrm{BZ}} \frac{d^2k}{V_{\mathrm{BZ}}}\, \delta[\omega - \epsilon(\mathbf{k})] = \frac{1}{2\pi^2 t} \mathrm{K}\left(\sqrt{1-\left(\frac{\omega}{4t}\right)^2}\right), \tag{16}$$

where $\mathrm{K}(\cdots)$ is the complete elliptic integral of first kind. As hopping parameter and unit of energy we choose $t \equiv 1$ in the following. The scattering amplitude for this system can be calculated in perturbation theory as

$$w(\mathbf{k}_0 \cdots \mathbf{k}_3) = \frac{2\pi}{{V_{\mathrm{BZ}}}^2} U^2 \delta_{\sigma_0\bar{\sigma}_1}\delta_{\sigma_2\bar{\sigma}_3}, \tag{17}$$

with the short-hand notation $\bar{\sigma}_i \equiv -\sigma_i$ for the BSE scattering rate Eq. (13), and

$$\tilde{w}(\epsilon_0 \cdots \epsilon_3) = 2\pi U^2 \delta_{\sigma_0\bar{\sigma}_1}\delta_{\sigma_2\bar{\sigma}_3} \tag{18}$$

for the case of BSE without **k** in Eq. (14), cf. Ref. [15].

In Fig. 1 we show the calculated scattering rates for different temperatures comparing DMFT and the BSE with and without momentum conservation. The quasiparticle renormalization is $Z \approx 1$ for these values of the interaction. In order to compare the structure of the scattering rates for different interaction strengths, we divide the scattering rate by U^2. The Boltzmann scattering rates then become completely independent of U. In contrast, the DMFT scattering rates depend on U in a nontrivial fashion (Fig. 1 shows $U = 1$ and $U = 2$) since it is a nonperturbative approach. Nonetheless, in the limit $U \to 0$, the DMFT normalized scattering rates must be U independent.

Comparing the DMFT scattering rates for both interaction strengths, one notices that the thus normalized scattering rates lie almost on top of each other for the inverse temperatures $\beta = 1.0$, $\beta = 2.5$, and $\beta = 20$, while they slightly deviate for $\beta = 0.5$, $\beta = 1.5$, and $\beta = 2.0$. Since there is a rather large uncertainty from the maximum entropy analytical continuation and the deviation is not systematic, we can conclude that the differences in the normalized DMFT scattering rates at $U = 1$ and $U = 2$ are within the error bars.

The scattering rates calculated by the BSE without **k** are in very good agreement with the DMFT data for all inverse temperatures except for $\beta = 1.0$. Again, this deviation may well originate from the uncertainties of the analytic continuation. In any case, the good agreement of the scattering rates from BSE without k and DMFT along with the $\sim U^2$ scaling of the DMFT results, clearly show that even at $U = 2t$ we are still in the perturbative regime. As we show in Appendix C, to second order in U the scattering rates as calculated in DMFT and BSE without **k** are indeed identical.

Note however that the spectral density [32] in Fig. 2 is already significantly smeared, especially at the band edges and the Van Hove singularity, because of the stronger interaction. This smearing is a direct consequence of the scattering rate in Fig. 1; and through the DMFT self-consistency it will in turn affect the scattering rates, but only in higher order in U (when self-consistently calculating the spectral function as indicated in Appendix C). This possibly explains why the BSE without **k** in Fig. 1 has a lower scattering rate at the band edge $\omega = \pm 4$

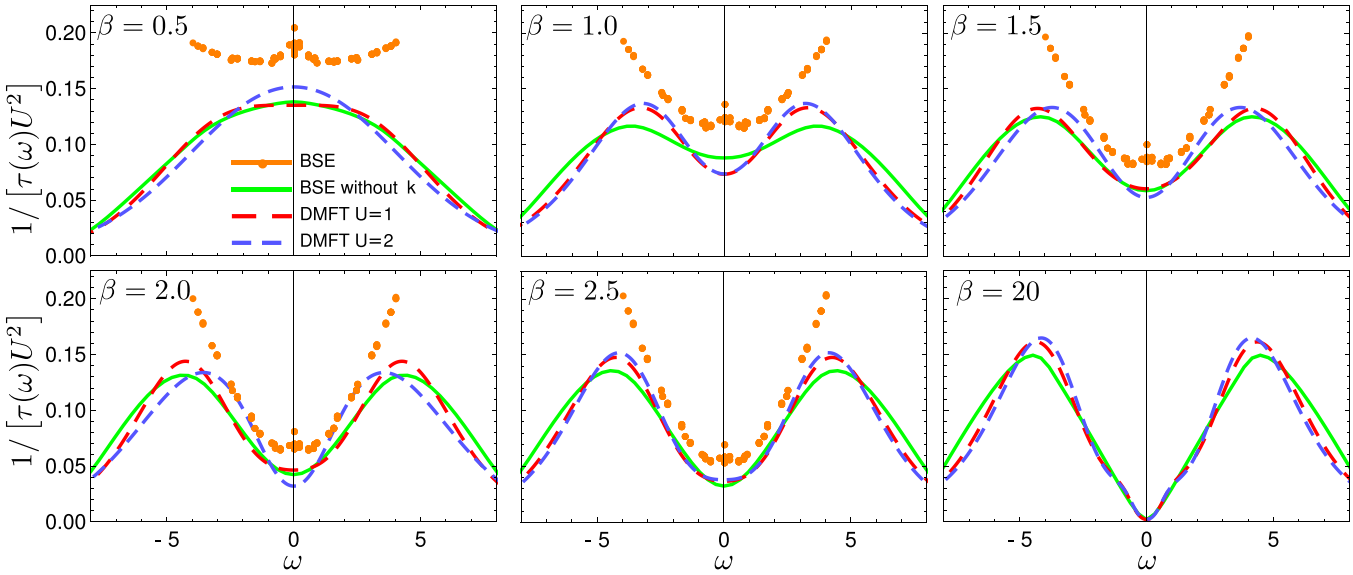

FIG. 1. Scattering rates $1/\tau$ normalized by the interaction squared (U^2) for the two-dimensional Hubbard model at half-filling calculated by DMFT and BSE with and without **k** conservation. The case $\beta = 20$ could not be calculated with full Boltzmann due to computational limitations. The scattering rates shown are the same for both spins in the paramagnetic phase.

and a larger one for larger $|\omega|$, albeit we cannot exclude this to be an artifact of the analytical continuation.

Both DMFT and BSE without **k** show a two-peak structure in the scattering rates with the peak positions roughly at the band edges. The width of these peaks increases with temperature. At the highest temperature ($\beta = 0.5$) there is only one peak visible which actually consists of the two peaks that are strongly overlapping. In Appendix B we show that the position of the two peaks can be approximately calculated from the first moment of the particle and hole density. The width and height of the peaks can be calculated when the zeroth and second moment of the particle density is taken into account in addition to the first moment.

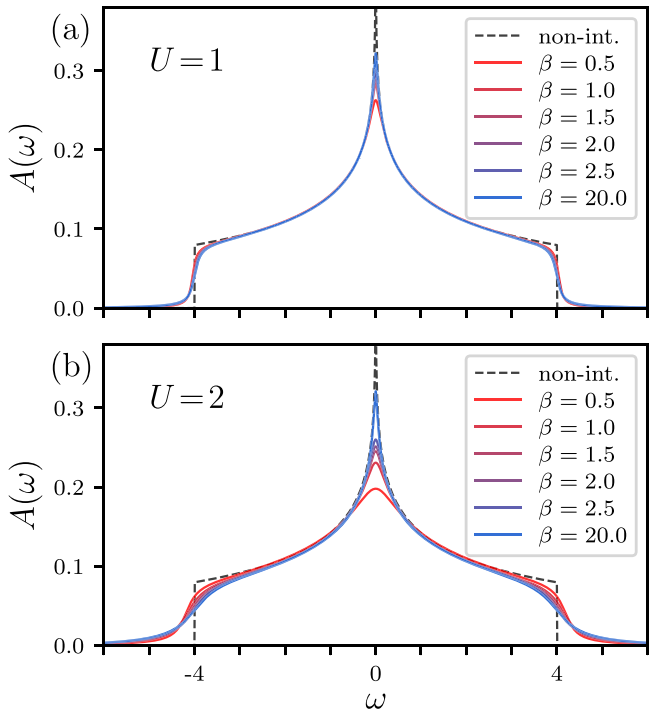

FIG. 2. DMFT spectral densities for (a) $U = 1$ and (b) $U = 2$ for different temperatures

After establishing a good agreement between DMFT and BSE without **k** at weak coupling, we next turn to the full BSE with momentum conservation. The thus calculated BSE scattering rates (dots in Fig. 1) deviate from the rates obtained with the other methods. First of all, as already mentioned, we highlight that several values, corresponding to different momenta, are present for each energy. Figure 1 shows a particularly strong spread at the Fermi level ($\omega = 0$). Furthermore, in contrast to BSE without **k** and DMFT, there are no scattering rates outside the noninteracting bandwidth ($|\omega| > 4$) any longer, as there is no momentum that has such an energy. This is in contrast to DMFT where, due to the aforementioned smearing of the band edges, such states exist. In BSE without **k**, even if no states exist outside the non-interacting bandwidth, the formula can still be meaningfully applied to calculate the scattering rates at those energies.

Another difference is that the BSE scattering rates are generally higher than DMFT or BSE without **k**, especially at the band edge ($|\omega| \lesssim 4$) and at higher temperatures also around the Fermi level ($\omega = 0$). As DMFT and BSE without **k** agree with each other, we can safely conclude that this difference originates from neglecting the momentum conservation of the scattering vertex. One can also smoothly interpolate between the results for the BSE with and without **k**, by replacing the momentum conserving δ function by a Gaussian and increasing its width (not shown here). The reason for these discrepancies is that the momentum averaged scattering amplitude does not take into account that there is, e.g., a particularly strong scattering among momenta at the van Hove singularities $(\pm\pi, 0)$ and $(0, \pm\pi)$. At low temperatures this scattering even leads to the formation of a pseudogap [33–40] which requires a beyond DMFT description [41–46].

A precursor thereof is visible here as the strong-momentum dependence of the scattering rate on the Fermi surface and a strong enhancement at the van Hove points. A similar enhanced scattering rate has been found for $\omega < \pi T$ but as a function of frequency at fixed momentum in second order PT [47,48].

IV. TWO-ORBITAL BAND INSULATOR

In this section we address the case of a band insulator in the weak to intermediate coupling regime. We consider a two-dimensional Hubbard-type model with two orbitals (A and B) at half-filling, i.e., $n = 2$ electrons per site in the two orbitals. This corresponds to $\mu = 0$ for our dispersion relation below. For simplicity we assume that electrons may only hop to neighboring orbitals of the same type and that the hopping amplitude has the same absolute size but opposite sign for both orbitals ($t_A = -1, t_B = 1 = t$). Furthermore, we add a local one-particle energy $\mp(\Delta/2 + 4t)$ for orbitals A and B, respectively. This results in a band gap of size Δ in the noninteracting DOS, with the top of the valence (A) band and the bottom of the conduction (B) band both at the Γ point. The interaction U is local and the same within and between both orbitals such that the interaction term of the Hubbard model acquires the simple form of Eq. (1).

We now discuss two different systems, one with $U = 4$ and one-particle gap $\Delta = 0$ and one with $U = 2$ and $\Delta = 2$. Due to the constant Hartree term in the self-energy, the effective gap in the interacting system is essentially the same $\Delta_{\text{eff}} \approx U + \Delta = 4$ for both setups. This is because at sufficiently low temperatures, orbital A is almost completely filled with two electrons per site and orbital B is empty. Hence an electron in orbital B perceives a Hartree energy $2U$ (interacts with both A electrons); an electron in orbital A instead has a Hartree energy $1U$ (as it only interacts with the electron of opposite spin in orbital A). The difference enlarges the band gap to $\Delta_{\text{eff}} = U + \Delta$.

The spectral densities for both cases are displayed in Fig. 3 and follow the above reasoning. At higher temperatures, we however induce holes in the valence and electrons in the conduction band. The difference in occupation is reduced, the band gap hence smaller. For the highest temperature ($\beta = 0.25$), the gap disappears completely for the case $U = 4$, $\Delta = 0$. The noninteracting DOS in Fig. 3 is constructed with the above enhanced effective band gap Δ_{eff} instead of Δ.

As this describes the DMFT spectrum at low temperatures reasonably well, we employ for the BSE the corresponding effective band structure

$$\epsilon_A(\mathbf{k}) = -\epsilon(\mathbf{k}) - \left(\frac{\Delta_{\text{eff}}}{2} + 4t\right), \tag{19}$$

$$\epsilon_B(\mathbf{k}) = \epsilon(\mathbf{k}) + \left(\frac{\Delta_{\text{eff}}}{2} + 4t\right), \tag{20}$$

where $\epsilon(\mathbf{k})$ is defined by Eq. (15). The corresponding DOS of the noninteracting system corrected by the Hartree shift is used for the BSE without $\mathbf{k}$ and given by

$$A_0^A(\omega) = A_0\left[\omega + \left(\frac{\Delta_{\text{eff}}}{2} + 4t\right)\right], \tag{21}$$

$$A_0^B(\omega) = A_0^A(-\omega), \tag{22}$$

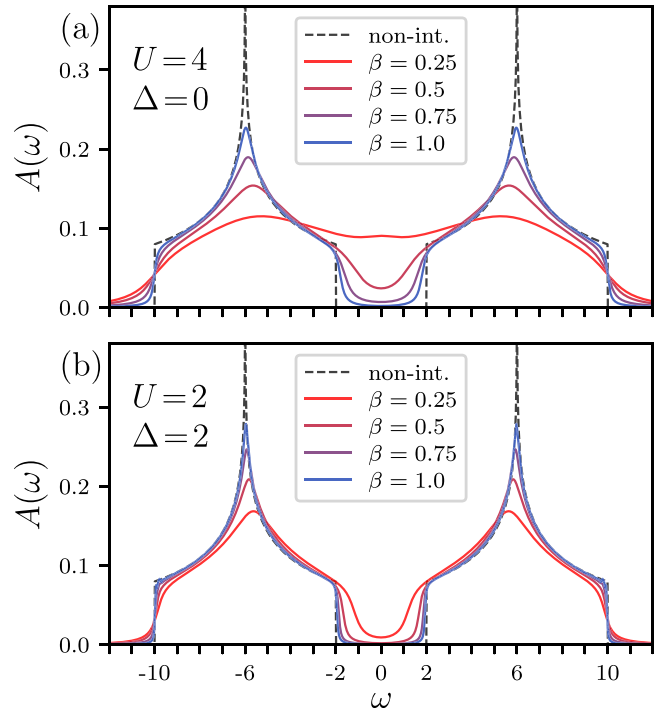

FIG. 3. Spectral densities for different temperatures for the case (a) $U = 4$, $\Delta = 0$ and (b) $U = 2$, $\Delta = 2$. For both cases, the effective band gap is $\Delta_{\text{eff}} \approx 4$.

with $A_0(\omega)$ defined in Eq. (16). Due to particle-hole symmetry and the simple form of the interaction, the BSE calculation can be simplified as outlined in Appendix D.

Figure 4 shows the scattering rate of the two-band system. The BSE with momentum conservation shows a seemingly parabolic increase starting with a sizable value at the lower band edge ($\omega = 2$). Superimposed on this trend is an enhanced scattering rate in the middle of the band at $\omega = 6$ with a strong momentum spread of the scattering rate. This is akin to the behavior at the Fermi level for the weakly correlated one-band Hubbard model in Fig. 1 and can again be attributed to the van Hove singularity.

Similar as for the one-band case, the scattering rates in BSE without $\mathbf{k}$ are slightly smaller than in the BSE with $\mathbf{k}$ conservation and already decay toward the upper band edge ($\omega = 10$). They closely resemble the DMFT values for the $U = 2$ case; only the peak of the scatterings is shifted to slightly higher energies than in DMFT. There are larger differences to the DMFT data at the intermediate coupling $U = 4$, which have systematically higher scattering rates at low energies. This is because stronger smearing of the spectral density at $U = 4$ leads to a smaller effective gap and some in-gap spectral weight, see Fig. 4. This, in turn, leads to more thermal excitations and therefore more scatterings. These effects can be included in BSE without $\mathbf{k}$ if we use the interacting spectral density $A^n(\omega)$ instead of the noninteracting one $A_0^n(\omega)$, which leads to a good agreement with the DMFT results, see Appendix E.

Eye catching is the strong suppression of the scattering rate upon decreasing temperature. The reason for this is the dramatic reduction of the number of thermally excited carriers which are needed to act as scattering partners. Note that with a

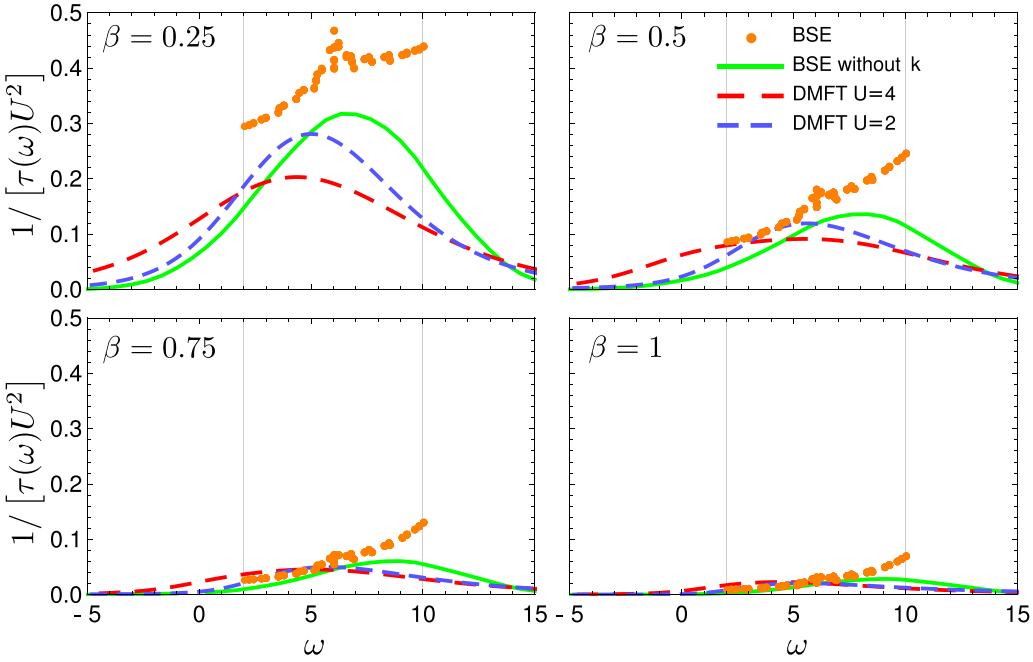

FIG. 4. Scattering rates normalized by the squared interaction for an electron in the upper band of a two-orbital band insulator as calculated with DMFT, BSE with and without **k**. Two different sets of parameters are used: $U = 4$, $\Delta = 0$ and $U = 2$, $\Delta = 2$. The gray, vertical lines indicate the band edges of the noninteracting system; the scattering rate for the lower band is particle-hole symmetric (mirrored around $\omega = 0$). Upon reducing temperature (increasing β) one can see that the scattering rate is strongly suppressed; for $\beta = 5$ (not shown) it is already of the order 10^{-6}. The reason for this is that the number of prospective scattering partners (available holes in the lower, electrons in the upper band) is exponentially decreasing with temperature.

density-density Coulomb interaction, the electron in the conduction (B) band either needs (i) another B electron to scatter with (the final state being again two B electrons), or (ii) a hole in the valence (A) band into which an A electron can scatter (final and initial state being one A and one B electron). Both B-electron and A-hole scattering partners however require thermally excited carriers. These are however exponentially suppressed at low temperatures, where we essentially have a completely filled lower band and a completely empty upper band. According to Eq. (13) this leads to a vanishing scattering rate.

V. STRONG COUPLING: MOTT INSULATOR

Finally, we compare the approaches introduced above in the strong coupling regime of the single-orbital Hubbard model. Since the BSE scattering rate is second order PT in the interaction, this is certainly the most problematic case for the BSE. For sufficiently large interaction, the noninteracting DOS splits into two, the upper and lower Hubbard band, see Fig. 5 (top). We have a Mott insulator, one of the cornerstones of strongly correlated electron systems [49].

If we use the BSE with the noninteracting DOS, this dramatic reshuffling of the DOS is not incorporated. The scattering rate is still the very same with a two peak structure as for weak coupling—just with the prefactor rescaled by U^2, see black-dotted line in Fig. 5. This kind of description assumes that we have a metal with states at low energies. It is not an appropriate description of a Mott insulator. Please note that the agreement of the peak position with that of DMFT

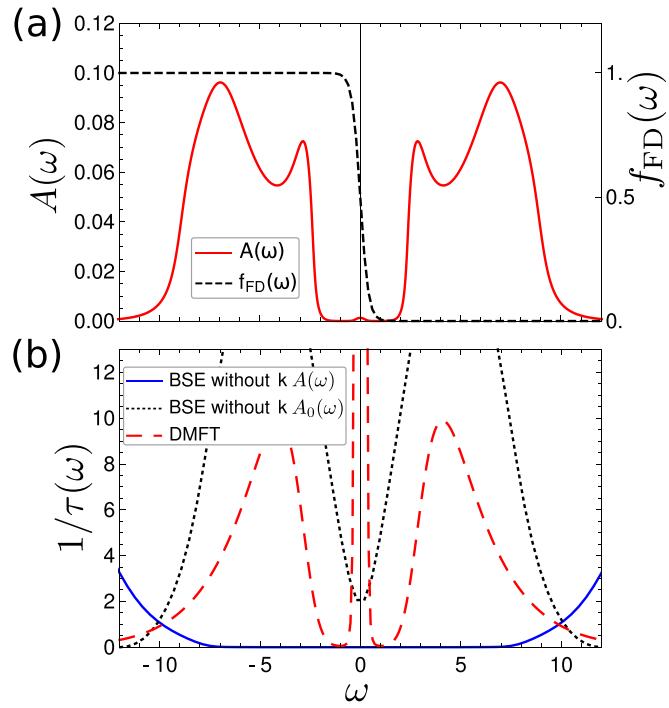

FIG. 5. (a) Spectral density as obtained by DMFT and Fermi-Dirac distribution for the case $U = 12$ and $\beta = 5$. (b) Scattering rates as obtained from DMFT, and BSE without **k** using either the noninteracting density of states [BSE without k $A_0(\omega)$] or the interacting DMFT spectral density shown [BSE without k $A(\omega)$].

is by chance since the latter changes with U, whereas the BSE peak originates from the noninteracting bandwidth and is independent of U (only the amplitude changes $\sim U^2$).

This problem can be mitigated if we consider better suited quasiparticles instead of the noninteracting ones. This is in general not trivial, and not always can proper quasiparticles with a long lifetime and weak interaction be identified. They might not even exist. Taking the electronic DMFT excitations of the Hubbard bands as our quasiparticles in the BSE without $\mathbf{k}$, we have to replace the noninteracting DOS $A_0(\omega)$ by the interacting spectral density $A(\omega)$ of Fig. 5 (top) in Eq. (14). Even if we have no well-defined quasiparticles, such a quantum Boltzmann description is possible [15] if we have a separation of timescales, and the average-time (distribution function) dynamics is slower than the relative-time dynamics. As was shown in Ref. [15], the thus modified BSE without $\mathbf{k}$ provides a good description of the DMFT impact ionization processes and redistribution of spectral weight in nonequilibrium [50].

Here we instead study in Fig. 5 (bottom, blue line) the one-particle scattering rates in the BSE without $\mathbf{k}$ and interacting $A(\omega)$: The Mott insulator is described as two split quasiparticle bands with the gap ~ 4 being much larger than temperature $T = 1/5$. Hence, if we add an extra electron in the upper Hubbard quasiparticle band it has no partners to scatter in BSE, the scattering rate is zero similar to the suppression of the scattering rate in the band insulator in Fig. 4. However, if the added electron has an excess energy ($\omega - \omega_{\mathrm{LBE}}$ relative to the lower band edge of the upper Hubbard band $\omega_{\mathrm{LBE}} \gtrsim 2$ in Fig. 5) which is larger than the Mott gap ($\Delta_{\mathrm{Mott}} \gtrsim 4$), i.e., $\omega \gtrsim 6$, impact ionization processes with an electron-hole excitation across the gap become possible. The phase space of such scattering processes increases quadratically with $\omega - \omega_{\mathrm{LBE}} - \Delta_{\mathrm{Mott}}$ for a box shaped DOS. This scattering stays intact (finite) even at low temperatures which is why our BSE scattering rates for the Mott insulator are larger than our BSE scattering rates for the band insulator if the temperature such as $T = 1/\beta = 1/5$ is sufficiently below the band gap.

Let us now turn to the DMFT scattering rates as extracted from the self-energy and shown in Fig. 5 (bottom, red-dashed line) [51]. The by far dominating feature (cut off by the finite y-axis scale) is at $\omega = 0$ where $\Sigma(\omega) = (U^2/4)\, 1/(\omega + i\alpha)$ in the large U limit of the Mott insulator with a Lorentzian broadening $\alpha \sim \pi T$. This pole is responsible for the splitting of the DOS into two Mott bands and yields the δ-like peak in $\mathrm{Im}\Sigma$ at $\omega = 0$. As a matter of course we cannot expect this feature to be described in the BSE without $\mathbf{k}$. It is also not necessary as $\omega = 0$ is in the middle of the Mott gap where there are essentially no states—essentially since at low temperature the aforementioned finite broadening leads to a very small spectral weight. This filling of the Mott gap with temperature [52] is a feature distinct from a band insulator. These in-gap states have an extremely short lifetime.

Let us now turn to the more relevant DMFT scattering rates within the Hubbard bands. These are orders of magnitude larger in DMFT than those from the BSE without $\mathbf{k}$ and with interacting $A(\omega)$. Also their shape is completely different: There is no suppression at the lower edge of the upper Hubbard bands which, as argued above, was the case if the scattering is due to impact ionization requiring a threshold energy; neither are the DMFT scattering rates flat or follow

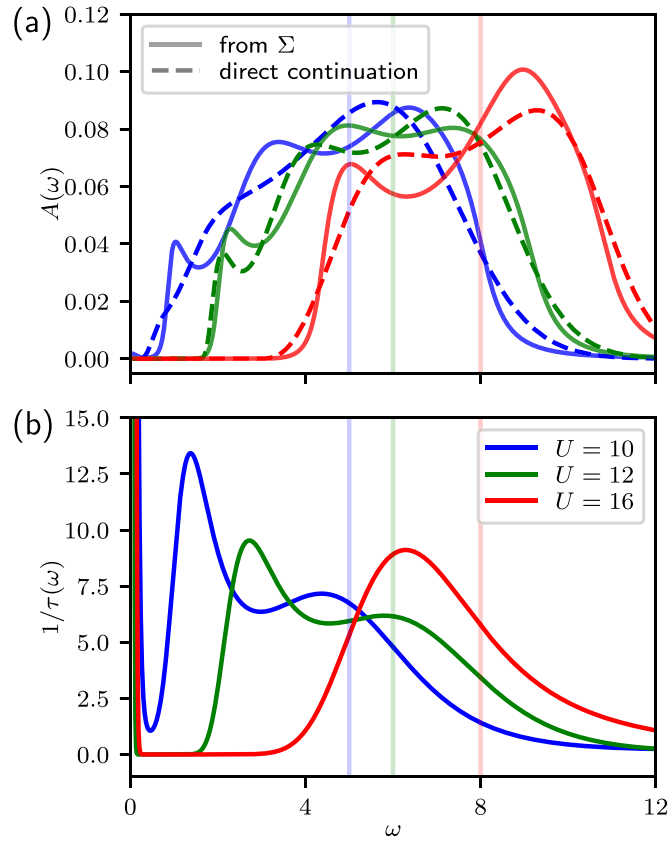

FIG. 6. (a) Spectral density as obtained by DMFT for $\beta = 10$ and different interaction strengths $U = 10$, 12, 16. The solid line $A(\omega)$'s are calculated from the analytically continued $\Sigma(\omega)$; the dashed lines are directly analytically continued from the Matsubara Green's function. (b) DMFT scattering rates for the same parameters as in (a).

the shape of the upper Hubbard band. Instead, the scattering rates are strongest around $\omega \sim 4$ close to the lower band edge, and are dramatically reduced for larger ω. Similar as the pole at $\omega = 0$, the maximum at $\omega \sim 4$ leads to a suppression of the spectral weight. Figure 5 (top), where we have calculated $A(\omega)$ from the analytically continued $\Sigma(\omega)$, even shows a two peak structure in the upper Hubbard band. Such a two peak structure was previously observed on the metallic side of the Mott transition, immediately before the quasiparticle peak vanishes [53–55]. On the Mott insulating side, Refs. [56,57] show an extra peak or a shoulder feature on the inner side of the Hubbard bands, similar to our findings. In Fig. 6 we also compare the $A(\omega)$ that is directly continued from the Green's function on the imaginary axis, which shows a shoulder rather than a double peak. While we hence cannot resolve within the maximum entropy uncertainty, whether we actually have a shoulder or double peak structure, it is clear that there is a feature in the upper Hubbard band. Mathematically, this is necessitated by the strong scattering rate in this region. A simple physical picture or understanding of these side structures in the Hubbard bands is still missing. Note that also in strong coupling perturbation theory to second order such a shoulder and hence asymmetry of the self-energy within the upper Hubbard band is observed [58], whereas the Hubbard-III

approximation [59] and the Falicov-Kimball model [60,61] do not show such a shoulder. In agreement, Fig. 6 shows this feature for different values of U. Since the scattering in BSE without $\mathbf{k}$ and with noninteracting $A_0(\omega)$ is merely rescaled by U^2, it is clear from Fig. 6 that the agreement of the position of the maximal scattering rate between BSE and DMFT in Fig. 5 (bottom, black-dotted vs red-dashed line) was by chance.

VI. DISCUSSION

In the following we will discuss two key findings in somewhat more detail.

(1) We have found that the DMFT scattering rate is much stronger and has a completely different shape than that obtained from the BSE without $\mathbf{k}$ for a Mott insulator (when using the Mott insulating interacting spectral function as a starting point for the BSE; the noninteracting DOS is clearly not appropriate). The reason for this is that the DMFT scattering rate is associated with the formation of the Hubbard bands ($\omega \sim 0$ peak of the scattering rate) and even side structures therein ($\omega \sim 4$ peak in Fig. 5). The Hubbard bands are created by the interaction of the very same electrons we also use as a test charge for calculating the scattering rate. If there is a local extra hole or electron, locally the Hubbard bands deform. Most noticeable this is in the filling of the Mott gap, which does not only occur with increasing temperature [52] but also if we drive the system out of equilibrium [15,16,62]. If we have an extra electron in a disordered spin background of the DMFT Mott insulator, it can or cannot hop to a neighboring site depending on the spin orientation of this neighbor. This leads to a large scattering rate without changing the number of double occupations. These processes are included in the DMFT but not in the BSE, they do not contribute to impact ionization (do not change the number of double occupations) or major energy redistributions.

For the BSE without $\mathbf{k}$ and with interacting (gapped) DOS, on the other hand, scattering processes are dominated by impact ionization and Auger processes, which are also included in DMFT but much weaker.

(2) Impact ionization corresponds to a process $c^\dagger_{iB\sigma} c_{iA\sigma} c^\dagger_{iB\bar{\sigma}} c_{iB\bar{\sigma}}$. That is, an electron in the upper band B scatters with an electron in the lower band A eventually leaving a hole in band A and two electrons in the upper band B. Here the initial electron needs sufficient energy for the second electron to be excited across the Mott gap. Auger processes are the particle-hole equivalent $c^\dagger_{iB\sigma} c_{iA\sigma} c^\dagger_{iA\bar{\sigma}} c_{iA\bar{\sigma}}$.

For a band insulator A and B are just the valence and conduction band. An interaction term of the form $H_X = U_{BABB} c^\dagger_{iB\sigma} c_{iA\sigma} c^\dagger_{iB\bar{\sigma}} c_{iB\bar{\sigma}}$ would mediate impact ionization but is not part of the density-density Coulomb interaction U of a two-orbital system, and is hence absent in our calculation. Even if we generalize the Coulomb interaction to the widely employed Kanamori form [63] with spin-flip and pair-hopping terms, there is no such term. Only the full Slater interaction [64,65] contains interaction terms that directly mediate such an impact ionization or Auger process. However, in realistic systems these interaction terms are very small or even vanish, which is the reason why they are often disregarded in the first place. Consider, e.g., a material with cubic symmetry and the orbitals $A = d_{xz}$ and $B = d_{xy}$. Then the interaction H_X for impact ionization (also sometimes called "correlated hopping") vanishes because the integral to calculate the matrix element U_{BABB} is odd under the transformation $z \to -z$ for the specific orbitals but also in many different situations; for a further going discussion, see, e.g., Refs. [66,67]. Even if it is not fully vanishing by symmetry, the matrix element U_{BABB} is much smaller than the density-density Coulomb interaction, because it involves the overlap between different orbitals A and B. A more viable route to enhance the scattering rate through impact or Auger processes in a band insulator is if the bands strongly hybridize so that the conduction and valence bands are admixtures of the A and B orbitals.

Now, let us turn to the Mott insulator. In this case one original band is split into lower and upper Hubbard bands by the Coulomb interaction U, i.e., the upper and lower Hubbard bands (A and B) still consist of the same orbital wave function. Hence in this case $U_{BABB} c^\dagger_{iB\sigma} c_{iA\sigma} c^\dagger_{iB\bar{\sigma}} c_{iB\bar{\sigma}}$ is just the local Hubbard interaction for an up and down spin of the same orbital $A = B$. This is why we needed to include impact ionization processes for the BSE without $\mathbf{k}$ description of the Mott insulator. Indeed this discussion further shows that impact ionization should be more relevant for a Mott than for a band insulator whenever we excite a particle at an energy ω sufficiently large to allow for an additional electron to transfer from the lower to the upper band [15,16,62,68,69]. This kind of impact ionization is not suppressed by lowering the temperature below the size of the gap, which is in contrast to the band insulator where the necessary Coulomb matrix elements are small.

(3) As a side note, this can also explain why the scattering rate for the band insulator preserves its two-bandlike structure even in the case $U = 4$, $\beta = 0.25$ when the spectral density does not show a gap any longer. The reason for this is again that the density-density interaction does not allow for impact excitation and Auger emission, which are very gap-size sensitive. Instead the scattering processes induced by the density-density interaction are agnostic about the gap size per-se. The additional B electron still needs another B (or A) electron to scatter with, and two empty final B states (or an empty A and an empty B state).

VII. CONCLUSION

We have studied and compared scattering rates using two widely employed methods: BSE which is equivalent to second order PT for the equilibrium scattering rate and DMFT. We have employed these methods out of their comfort zone, where they cannot be applied with mathematical rigor. For DMFT this is the dimensionality of the systems studied (2D), which is far away from the limit of infinite dimensions where DMFT become exact. For the BSE or second order PT it is the strong interaction regime of the Mott insulator, where a rate equation with perturbatively determined scattering rates cannot safely be applied. We have mitigated the latter in part by using the interacting spectral function instead of the noninteracting DOS as the quasiparticle states whose occupation dynamics (here scattering rate) is calculated by BSE.

DMFT somewhat underestimates the scattering rates and by construction cannot resolve their momentum, only their energy dependence. The momentum dependence is particularly

strong in the middle of the band where the Van Hove singularity is located. The physical reason behind both discrepancies is that the phase space for the scattering of a quasiparticle with another quasiparticle explicitly depends on available unoccupied states linked by momentum conservation. If we replace the momentum-conserving δ function by a Gaussian with increasing width or directly disregard momentum conservation in the BSE without $\mathbf{k}$, the scattering rates are reduced and the DMFT results reproduced by BSE without $\mathbf{k}$ for the weakly correlated metal ($U = 1$ or 2).

The biggest challenge for the BSE is the strongly interacting Mott insulating state. Here the DOS is split into two Hubbard bands which we take as the starting quasiparticle DOS in the BSE without $\mathbf{k}$. In the BSE, the scattering rate is due to impact ionization. These processes are well described and in good agreement with DMFT [15]. However, in DMFT additional scattering processes which can be associated with the formation of the Hubbard bands and shoulders therein dominate. The same specimen of electrons that through their interaction form the Hubbard bands are also added as a charge probe, locally disturbing the spectrum. These huge DMFT scattering rates are beyond a BSE description with a static DOS.

Scattering in an interacting band insulator bears no similarity at all with that in the Mott insulator. It is strongly suppressed at low temperatures since scattering is only possible if there are thermal excitations across the gap. BSE without $\mathbf{k}$ and DMFT agree, while the BSE with momentum conservation has, similar as for the weakly correlated metal, somewhat larger scattering rates. The difference to the Mott insulator does not only lie in the huge scattering associated with the Hubbard bands (which makes the DMFT scattering rate much larger than that of BSE), but also in the absence of impact ionization which dominates the scattering in BSE for a Mott insulator.

Impact ionization describes a process where one electron in the upper band scatters with an electron in the lower band, with the final state being two electrons in the upper band and a hole in the lower band. Auger processes are related through a particle-hole transformation. For the considered density-density interaction such processes are not possible directly for a band insulator and have hence not been considered. In contrast in a Mott insulator they are possible because the upper and lower band are made up from the very same physical orbital, so that the density-density interaction of this orbital directly generates impact ionization and Auger processes. For a band insulator, these processes are mediated by a different element of the Coulomb matrix (coined "correlated hopping"), which is typically much smaller or even zero. Alternatively, also a sizable hybridization between valence and conduction band can lead to impact ionization. Notwithstanding, since the correlated hopping is much smaller than the density-density interaction, Mott insulators appear to be better suited than band insulators for increasing the efficiency of solar cells through impact ionization [15,16,62,68–71].

ACKNOWLEDGMENTS

We thank M. Eckstein, A. Kauch, C. Watzenböck, and P. Werner for discussions, and acknowledged financial support from the Austrian Science Fund (FWF) through the Doctoral School W1243 Solids4Fun (Building Solids for Function, M.W.) and project P30997 (M.W., J.K., K.H.), and from Nanyang Technological University, NAP-SUG (M.B.). Calculations have been done in part on the Vienna Scientific Cluster (VSC).

APPENDIX A: SCATTERING RATE FROM THE RETARDED GREEN'S FUNCTION

1. Derivation of the formula

If we linearize the self-energy around the (real part of the) pole $\tilde{\epsilon}(\mathbf{k}) = Z[\epsilon(\mathbf{k}) + \mathrm{Re}\Sigma_R(0) - \mu]$ we get Eq. (7) whose Fourier transformation is

$$G(\mathbf{k}, t) = \frac{1}{2\pi}\int_{-\infty}^{\infty} d\omega \frac{Ze^{-i\omega t}}{\omega - \tilde{\epsilon}(\mathbf{k}) - Z\mathrm{Im}\Sigma_R(\omega)}. \tag{A1}$$

Note that a linearization of the self-energy around $\omega = 0$ might not be justified any longer if the pole is at large frequencies and that there may be more than one pole at a given $\mathbf{k}$. For example, for the Mott insulator we have two poles for each $\mathbf{k}$. However, this merely means that we have $\mathrm{Re}\Sigma_R(\tilde{\epsilon})$ instead of $\mathrm{Re}\Sigma_R(0)$ and that we have a sum of poles in Eq. (A1) instead of a single one, respectively. With these modifications we can use the same procedure as discussed in the following for a single pole.

The integral (A1) can be solved by closing the contour on the lower complex half-plane of frequencies (since $t > 0$ the integrand is exponentially suppressed here). Then Eq. (A1) can be computed by the residue theorem. The pole is at $[\mathrm{Re}\omega_p, \mathrm{Im}\omega_p] = \{\tilde{\epsilon}(\mathbf{k}), Z\mathrm{Im}\Sigma[\omega_p \approx \tilde{\epsilon}(\mathbf{k})]\}$. Here, in principle, $\mathrm{Im}\omega_p$ would have to be obtained self-consistently, but if $\mathrm{Im}\Sigma$ is small we can (approximately) calculate it using only the real part of the pole. The residue theorem then yields for the integral in Eq. (A1)

$$2\pi i \lim_{\omega\to\omega_p}(\omega - \omega_p)\frac{Ze^{-i\omega t}}{\omega - \tilde{\epsilon}(\mathbf{k}) - Z\mathrm{Im}\Sigma_R(\tilde{\epsilon})} \propto e^{-it\tilde{\epsilon}}e^{tZ\mathrm{Im}\Sigma_R(\tilde{\epsilon})}; \tag{A2}$$

or for the probability to find a particle that is added at time 0 to the quasiparticle state $\mathbf{k}$ still in this state at a later time t:

$$|G_R(\mathbf{k}, t)|^2 \propto e^{2Z\mathrm{Im}\Sigma_R[\tilde{\epsilon}(\mathbf{k})]t}, \tag{A3}$$

which yields the (inverse) lifetime Eq. (8).

2. Analytic example

It is instructive to consider an example where everything can be computed exactly, such that we can test the above approximations. We consider a self-energy of the form

$$\Sigma(\omega) = A\left(\frac{1}{\omega - E + i\alpha} + \frac{1}{\omega + E + i\alpha}\right). \tag{A4}$$

For parameters $A = 0.1$, $E = 4$, $\alpha = 1.5$ it is very similar in size and shape to our results for the single-orbital weak coupling results for $\beta \approx 2$, as shown in Fig. 7.

If we insert this self-energy together with $\mu = 0$ into the Green's function Eq. (6), the locations of the poles are determined by a cubic equation in ω. It is possible to solve this

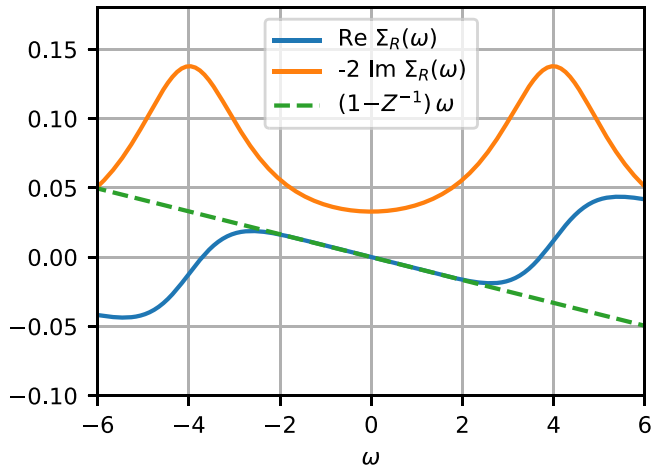

FIG. 7. Model self-energy of Eq. (A4) for $A = 0.1$.

equation analytically for arbitrary parameters. Notably, the pole locations will depend on $\epsilon(\mathbf{k})$. The locations of the poles in dependence of ϵ are shown in Fig. 8, and for a larger value of $A = 0.8$ in Fig. 9. Pole 2 is the one we usually associate with the quasiparticle.

Now it is possible to compute the time-dependent Green's function exactly by evaluating the Fourier integral in Eq. (A1). The results for a few different values of ϵ are shown as solid lines in Fig. 10. Given the exact $G(t)$ as a reference, we show the contribution of the residue of the pole (pole 2) that is closest to the real axis, Eq. (A2) as dashed lines. Finally we also show the exponential decay where the scattering rate was approximated by the imaginary part of the self-energy. Clearly for small values of ϵ this is an excellent approximation. Closer to the band edge it does not match so well any more, especially in the case of the large self-energy (large A; right panel). This mismatch may already be anticipated when looking at Fig. 9.

APPENDIX B: CONVOLUTION METHOD

For the case of a single band at half-filling, we here reformulate the expression for the scattering rate in BSE without $\mathbf{k}$, Eq. (14), to gain some further analytical insight. To this end, we define the particle density as $n_p(\omega) \equiv f_{\mathrm{FD}}(\omega)A_0(\omega)$ and the hole-density as $n_h(\omega) \equiv [1 - f_{\mathrm{FD}}(\omega)]A_0(\omega)$. With these definitions and the scattering amplitude for the one-band system introduced in Sec. III we may rewrite Eq. (14) as

$$\frac{1}{\tau_n(\epsilon_0)} = 2\pi U^2 \int d\epsilon_1 d\epsilon_2 d\epsilon_3 [\delta(\epsilon_0 + \epsilon_1 - \epsilon_2 - \epsilon_3) \times (n_h(\epsilon_1)n_p(\epsilon_2)n_p(\epsilon_3) + n_p(\epsilon_1)n_h(\epsilon_2)n_h(\epsilon_3))]. \tag{B1}$$

For a system with particle-hole symmetry it holds that $n_p(\omega) = n_h(-\omega)$. Using this property and the definition of the convolution $(a * b)(\omega) \equiv \int d\tilde{\omega}\, a(\omega - \tilde{\omega})b(\tilde{\omega})$, Eq. (B1) can be further reduced to

$$\frac{1}{\tau_n(\omega)} = 2\pi U^2 [g(\omega) + g(-\omega)], \tag{B2}$$

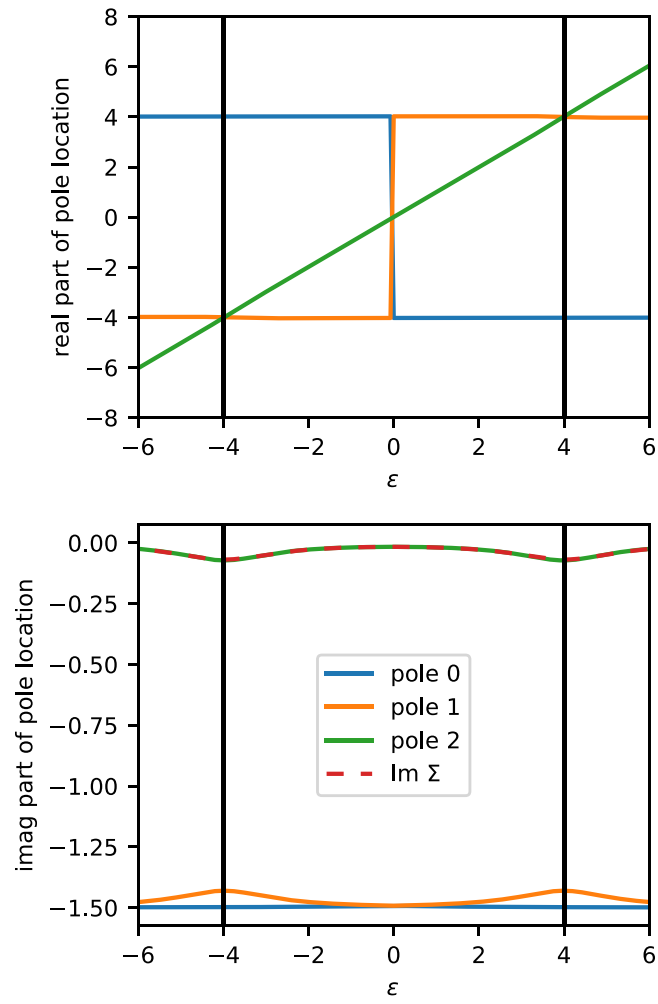

FIG. 8. Pole locations with model self-energy. Clearly the imaginary part of the location of the pole with the smallest imaginary part (pole 2) agrees well with the imaginary part of the self-energy $\mathrm{Im}\Sigma(\omega = \tilde{\epsilon})$. The imaginary parts of the other two poles are much larger. $Z \approx 0.99$ for this case.

with

$$g(\omega) \equiv (n_p * n_p * n_p)(\omega). \tag{B3}$$

The above equation states that the scattering rate consists of the sum of the particle density convoluted with itself twice, and its mirrored version.

According to the central limit theorem [72], a function with compact support becomes a Gaussian function in the limit when it is convoluted an infinite times with itself. If the particle-density is smooth, the result after two convolutions with itself is already very similar to a Gaussian, see Fig. 11(a).

This allows us to further reduce complexity and increase understanding: A general Gaussian function, i.e.,

$$f_{\mathrm{gauss}}(\omega) \equiv \frac{\alpha}{\sigma\sqrt{2\pi}} \exp\left[-\frac{(\omega - \omega_0)^2}{2\sigma^2}\right] \tag{B4}$$

is completely defined by three parameters: its integral value α, its variance σ^2, and its zero-point ω_0. For a given Gaussian

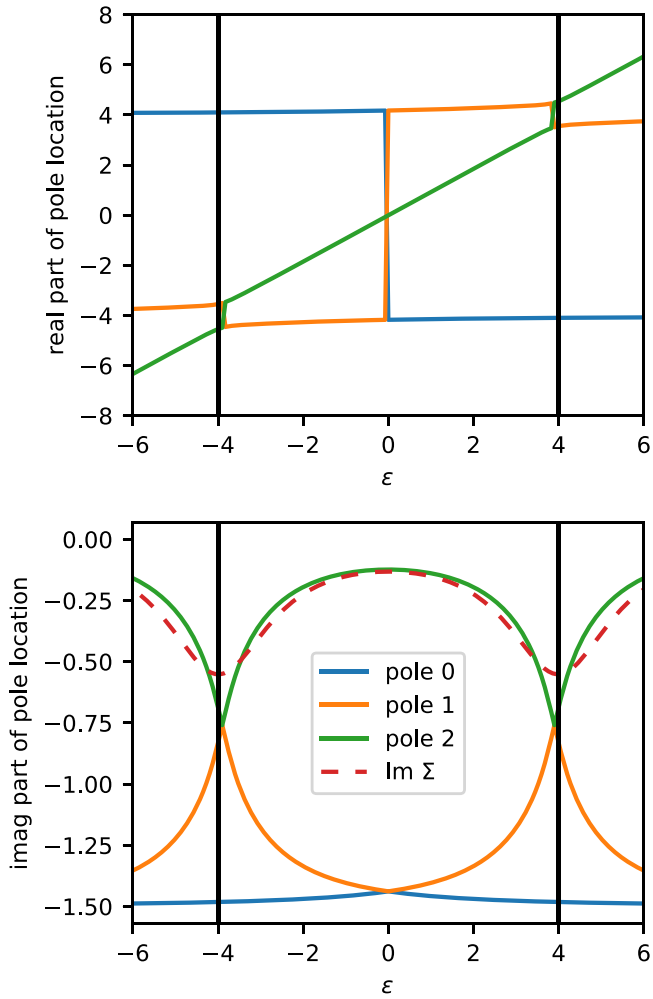

FIG. 9. Same as Fig. 8 but with A increased by a factor of 8. Also here the imaginary part of the location of the pole with the smallest imaginary part is similar to the imaginary part of the self-energy, but not in quantitative agreement. At the band edge, a second pole is of similar size and will thus have considerable influence on the scattering rate. $Z \approx 0.94$ for this case.

these three parameters can be calculated from its zeroth, first, and second moment,

$$\alpha = F_0[f_{\text{gauss}}], \tag{B5}$$

$$\omega_0 = \frac{F_1[f_{\text{gauss}}]}{F_0[f_{\text{gauss}}]}, \tag{B6}$$

$$\sigma^2 = \frac{F_2[f_{\text{gauss}}]}{F_0[f_{\text{gauss}}]} - \left(\frac{F_1[f_{\text{gauss}}]}{F_0[f_{\text{gauss}}]}\right)^2, \tag{B7}$$

where $F_n[f]$ is the nth moment of the function $f(\omega)$, i.e.,

$$F_n[f] \equiv \int d\omega f(\omega)\omega^n. \tag{B8}$$

We can now approximate the function $g(\omega)$ with a Gaussian function by calculating the parameters α, ω_0, and σ from its moments using Eqs. (B5)–(B7) with g instead of f_{gauss}. The function $g(\omega)$ is calculated from a convolution of the particle density, hence, the moments of $g(\omega)$ can be directly inferred from the moments of the particle-density $n_p(\omega)$,

$$F_0[g] = (F_0[n_p])^3, \tag{B9}$$

$$F_1[g] = 3F_1[n_p](F_0[n_p])^2, \tag{B10}$$

$$F_2[g] = 3[F_2[n_p](F_0[n_p])^2 + 2(F_1[n_p])^2 F_0[n_p]]. \tag{B11}$$

With the Eqs. (B5)–(B7) and the Eqs. (B9)–(B11) the parameters for the Gaussian function can eventually be calculated from the moments of particle density as

$$\alpha = (F_0[n_p])^3, \tag{B12}$$

$$\omega_0 = 3\frac{F_1[n_p]}{F_0[n_p]}, \tag{B13}$$

$$\sigma^2 = 3\left[\frac{F_2[n_p]}{F_0[n_p]} - \left(\frac{F_1[n_p]}{F_0[n_p]}\right)^2\right], \tag{B14}$$

and the scattering rate may be approximated as

$$\left(\frac{1}{\tau(\omega)}\right)_{\text{gauss}} \equiv 2\pi U^2[f_{\text{gauss}}(\omega) + f_{\text{gauss}}(-\omega)]. \tag{B15}$$

Figure 11(b) shows that this approximate Gaussian agrees with the exact BSE without **k** scattering rate to very good approximation. This explains the origin of the maximal scattering rate and why this maximum lies within the bandwidth of the DOS not at its edge as in the BSE with **k**.

APPENDIX C: CONNECTION TO SECOND ORDER PERTURBATION THEORY

The scattering rate of Eq. (B1) is actually that of second order PT. Let us discuss this connection here for the less familiar equilibrium scattering rate calculated in BSE without **k** by Eq. (B1) and second order iterated perturbation theory (IPT) [7,73,74] as the prototypical second order PT for DMFT. In IPT, the DMFT self-energy is calculated in second order in U from the impurity Green's function $\mathcal{G}$. Directly on the real frequency axis and in terms of the impurity spectral function $\mathcal{A}(\omega) = -1/\pi\ \text{Im}\mathcal{G}(\omega)$ the IPT self-energy reads (see, e.g., Eq. (22) in [75] where ϵ_1 and ϵ_2 are exchanged)

$$\Sigma_R(\omega) = \lim_{\alpha\to 0} U^2 \int d\epsilon_1 d\epsilon_2 d\epsilon_3 \mathcal{A}(\epsilon_1)\mathcal{A}(\epsilon_2)\mathcal{A}(\epsilon_3) \times \frac{f_{\text{FD}}(-\epsilon_1)f_{\text{FD}}(\epsilon_2)f_{\text{FD}}(\epsilon_3) + f_{\text{FD}}(\epsilon_1)f_{\text{FD}}(-\epsilon_2)f_{\text{FD}}(-\epsilon_3)}{\omega + i\alpha + \epsilon_1 - \epsilon_2 - \epsilon_3}. \tag{C1}$$

With $f_{\text{FD}}(-\epsilon) = 1 - f_{\text{FD}}(\epsilon)$ and $\lim_{\alpha\to 0} \text{Im}1/(\omega + \epsilon_1 - \epsilon_2 - \epsilon_3) = -\pi\delta(\omega + \epsilon_1 - \epsilon_2 - \epsilon_3)$ this yields Eq. (B1) or (14) if we replace $\mathcal{A}(\epsilon)$ by $A_0(\epsilon)$ which is possible to lowest order in U or the first iteration of the IPT. Through the DMFT self-consistency condition [9,76] $\mathcal{G}(\omega)^{-1} = G(\omega)^{-1} + \Sigma(\omega)$, $\mathcal{A}(\epsilon)$ is updated in subsequent iterations. Equation (C1) also shows that there is no momentum conservation at the scattering when we calculate the self-energy: simply replace the local Σ_R and $A(\epsilon)$'s by their Fourier transformed **k** sum. Each momentum sum transforms independently of the others, there is no momentum conservation.

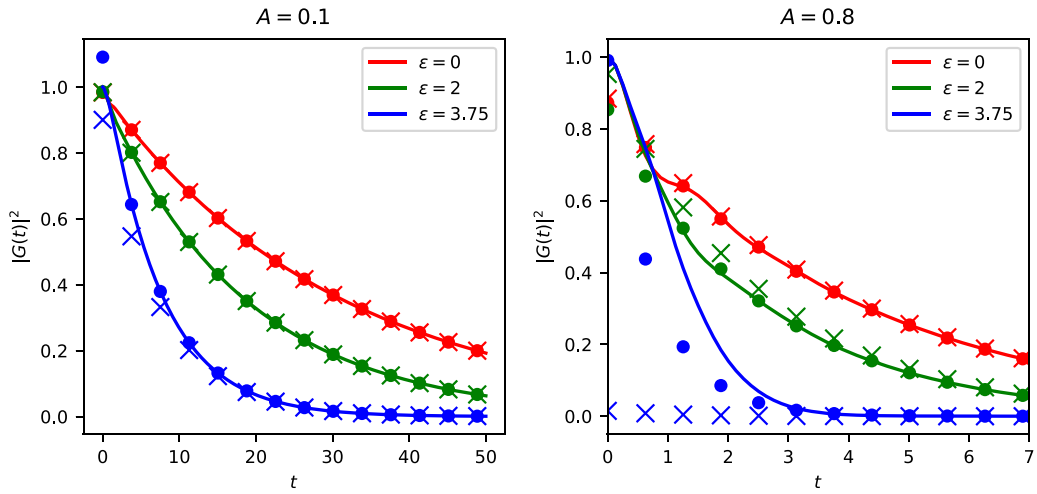

FIG. 10. Absolute square of the time-dependent Green's function for the model self-energy with $A = 0.1$ (left) and $A = 0.8$ (right). Solid lines are time-dependent Green's functions that are computed by Eq. (A1). Dots show the contribution of the residue at the pole with smallest $|\mathrm{Im}\hat{\omega}|$. Crosses show the approximation given by Eq. (A3).

APPENDIX D: SIMPLIFICATIONS FOR THE TWO-ORBITAL CASE DUE TO PARTICLE-HOLE SYMMETRY

In this Appendix we discuss some simplifications that are possible due to particle-hole symmetry and a density-density interaction U which is the same for all orbitals. Indeed, the scattering rate can be actually calculated from a single band in BSE. The reason for this is as follows: For the BSE with momentum conservation the scattering rate in the upper band reads

$$\begin{aligned}\frac{1}{\tau_B(\mathbf{k}_0)} = 6\pi U^2 \frac{1}{{V_{BZ}}^2} \int d^2k_1 d^2k_2 d^2k_3 \\ \times [\delta[\epsilon_B(\mathbf{k}_0) + \epsilon_B(\mathbf{k}_1) - \epsilon_B(\mathbf{k}_2) - \epsilon_B(\mathbf{k}_3)] \\ \times \sum_{\mathbf{G}} \delta(\mathbf{k}_0 + \mathbf{k}_1 - \mathbf{k}_2 - \mathbf{k}_3 + \mathbf{G}) \\ \times (\{1 - f_{\mathrm{FD}}[\epsilon_B(\mathbf{k}_1)]\} f_{\mathrm{FD}}[\epsilon_B(\mathbf{k}_2)] f_{\mathrm{FD}}[\epsilon_B(\mathbf{k}_3)] \\ + f_{\mathrm{FD}}[\epsilon_B(\mathbf{k}_1)]\{1 - f_{\mathrm{FD}}[\epsilon_B(\mathbf{k}_2)]\} \\ \times \{1 - f_{\mathrm{FD}}[\epsilon_B(\mathbf{k}_3)]\})], \end{aligned} \tag{D1}$$

and for the BSE without $\mathbf{k}$ case it reads

$$\begin{aligned}\frac{1}{\tau_B(\epsilon_0)} = 6\pi U^2 \int d\epsilon_1 d\epsilon_2 d\epsilon_3 \\ \times \big[\delta(\epsilon_0 + \epsilon_1 - \epsilon_2 - \epsilon_3) A_0^B(\epsilon_1) A_0^B(\epsilon_2) A_0^B(\epsilon_3) \\ \times ([1 - f_{\mathrm{FD}}(\epsilon_1)] f_{\mathrm{FD}}(\epsilon_2) f_{\mathrm{FD}}(\epsilon_3) \\ + f_{\mathrm{FD}}(\epsilon_1)[1 - f_{\mathrm{FD}}(\epsilon_2)][1 - f_{\mathrm{FD}}(\epsilon_3)])\big]. \end{aligned} \tag{D2}$$

Due to particle-hole symmetry it further holds that $1/\tau^A(-\omega) = 1/\tau^B(\omega) \equiv 1/\tau(\omega)$. The multiplicative factor of 3 compared to the one-band case (Sec. III) in the scattering amplitude reflects the different scattering processes an electron in the upper band may perform: an electron with a certain spin σ in band B may scatter with an an electron $B\bar{\sigma}$, $A\sigma$, and $A\bar{\sigma}$. Since the density-density interaction does not allow for spin flips and pair hopping nor impact excitation which would require an interaction of the form $c^\dagger_{iB\bar{\sigma}} c_{iA\bar{\sigma}}$ $c^\dagger_{iB\sigma} c_{iB\sigma}$ nor Auger excitations, there are no further allowed processes to be taken into account. Since the interaction between the bands is the same as within the bands ($U = V$), all scattering processes have the same scattering amplitude $\propto 2\pi U^2$ ($\propto 2\pi \frac{1}{{V_{BZ}}^2} U^2$), eventually leading to $\propto 3 \times 2\pi U^2 = 6\pi U^2$ ($\propto 6\pi \frac{1}{{V_{BZ}}^2} U^2$).

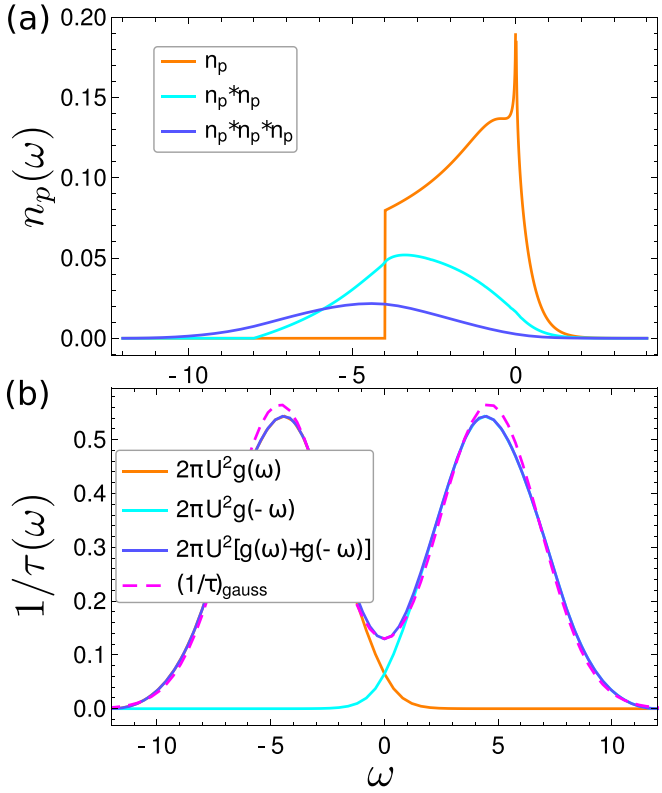

FIG. 11. (a) Particle-density n_p and the particle-density convoluted one and two times with itself. (b) Scattering rate in BSE without $\mathbf{k}$ calculated with the convolution method compared to the approximated scattering rate that consists of two Gaussian functions.

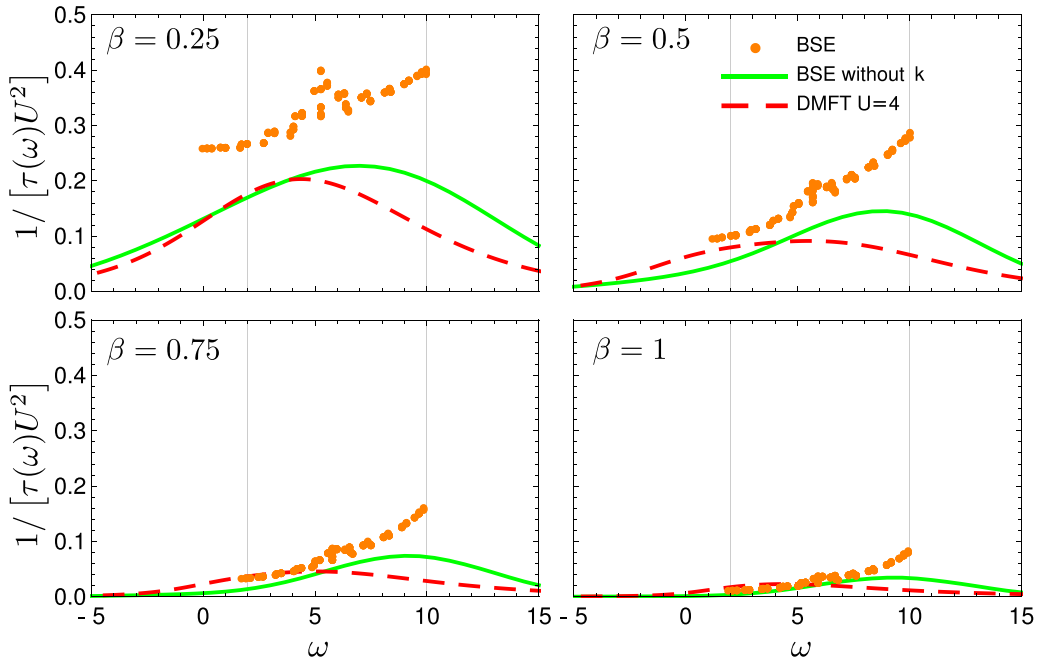

FIG. 12. Scattering rate normalized by U^2 for the two-band case with $U = 4$. Same as Fig. 4 but using the interacting DMFT spectral density $A(\omega)$ instead of $A_0(\omega)$ in Eqs. (21) and (22) for the BSE without **k**. For the BSE with momentum conservation the dispersion and gap has been adapted to the DMFT as well. Using the interacting spectral function leads to a better agreement with DMFT.

APPENDIX E: BAND INSULATOR WITH RENORMALIZED BANDS

As already mentioned in Sec. IV, the deviation of BSE without **k** and DMFT can be reduced by using the interacting spectral density instead of the noninteracting DOS [$A_0(\omega) \to A(\omega)$ in Eq. (D2)]. For the theoretical justification and background of this procedure, see Ref. [15].

For the band insulator, the main difference between $A_0(\omega)$ and $A(\omega)$ is that thermal excitations across the gap reduce the difference in Hartree energy and hence the band gap. Moreover, with more thermal excitations there are more particles an electron or hole can scatter with. Hence the scattering rate is enhanced, which in turn leads to broadening effects in $A(\omega)$, visible in Fig. 3 at the band edges and the van Hove singularity.

In order to make all methods comparable, we are also using a renormalized band for the BSE with momentum conservation. For that purpose we calculate the momentum-dependent spectral density $A_{\mathbf{k}}(\omega)$ and then extract for each given momentum the corresponding energy where the spectral density has its maximum. In this way one can obtain a renormalized dispersion relation which we then use for the calculation of the scattering rate.

Figure 12 shows the thus obtained BSE results at $U = 4$ with and without momentum conservation; the DMFT result is the same as in Fig. 4. Using the interacting spectral function and correspondingly renormalized band structure, reduces the scattering rate in the middle of the upper band at $\omega \sim 6$. In contrast, the scattering rate at small $\omega \sim 0$ is enhanced at high temperatures. Here the interacting spectrum has states in the (pseudo)gap. Overall, using the interacting DOS as a starting point, the BSE can explain most changes of the $U = 4$ DMFT scattering rate compared to $U = 2$.

[1] M. Grioni, J. Electron Spectrosc. Relat. Phenom. **117–118** (2001), special issue on correlated electron systems.
[2] A. Damascelli, Z. Hussain, and Z.-X. Shen, Rev. Mod. Phys. **75**, 473 (2003).
[3] P. Drude, Ann. Phys. **308**, 369 (1900).
[4] P. Drude, Ann. Phys. **306**, 566 (1900).
[5] Both in dynamical mean-field theory and Boltzmann there are no vertex corrections to the optical conductivity.
[6] W. Metzner and D. Vollhardt, Phys. Rev. Lett. **62**, 324 (1989).
[7] A. Georges and G. Kotliar, Phys. Rev. B **45**, 6479 (1992).
[8] M. Jarrell, Phys. Rev. Lett. **69**, 168 (1992).
[9] A. Georges, G. Kotliar, W. Krauth, and M. J. Rozenberg, Rev. Mod. Phys. **68**, 13 (1996).
[10] L. Boltzmann, Sitzungsberichte Kaiserlichen Akad. Wissensch. **66**, 275 (1872).
[11] D. W. Snoke, *Solid State Physics Essential Concepts*, 1st ed. (Pearson Education, London, 2007).
[12] J. Ziman, *Electrons and Phonons: The Theory of Transport Phenomena in Solids* (Oxford University Press, Oxford, 1960).
[13] R. G. Chambers, *Electrons in Metals and Semiconductors* (Chapman and Hall, Englewood Cliffs, NJ, 1990).
[14] For an overview of the Mott-Hubbard transition and the physics of the Mott insulator see [49].

[15] M. Wais, M. Eckstein, R. Fischer, P. Werner, M. Battiato, and K. Held, Phys. Rev. B **98**, 134312 (2018).

[16] P. Werner, K. Held, and M. Eckstein, Phys. Rev. B **90**, 235102 (2014).

[17] A. A. Abrikosov, L. P. Gorkov, and I. E. Dzyaloshinski, *Methods of Quantum Field Theory in Statistical Physics* (Dover, New York, 1975).

[18] K. Held, Adv. Phys. **56**, 829 (2007).

[19] W. Nolting, *Grundkurs Theoretische Physik 7: Viel-Teilchen-Theorie* (Springer Spektrum, Berlin, 2015).

[20] T. Matsubara, Prog. Theor. Phys. **14**, 351 (1955).

[21] E. Gull, A. J. Millis, A. I. Lichtenstein, A. N. Rubtsov, M. Troyer, and P. Werner, Rev. Mod. Phys. **83**, 349 (2011).

[22] J. Kaufmann, P. Gunacker, A. Kowalski, G. Sangiovanni, and K. Held, Phys. Rev. B **100**, 075119 (2019).

[23] N. Parragh, A. Toschi, K. Held, and G. Sangiovanni, Phys. Rev. B **86**, 155158 (2012).

[24] N. Parragh, A. Toschi, K. Held, and G. Sangiovanni, in [23], p. 155158.

[25] M. Jarrell and J. E. Gubernatis, Phys. Rep. **269**, 133 (1996).

[26] D. Geffroy, J. Kaufmann, A. Hariki, P. Gunacker, A. Hausoel, and J. Kuneš, Phys. Rev. Lett. **122**, 127601 (2019).

[27] J. Kaufmann, ana_cont: Package for analytic continuation of many-body Green's functions, https://github.com/josefkaufmann/ana_cont (2020).

[28] M. Wais, K. Held, and M. Battiato, Comput. Phys. Commun. **264**, 107877 (2021).

[29] S. Ono, Phys. Rev. B **97**, 054310 (2018).

[30] S. Ono and T. Suemoto, Phys. Rev. B **102**, 024308 (2020).

[31] A. A. Katanin, V. Y. Irkhin, and P. A. Igoshev, *Model'nye Podhody k Magnetizmu Dvumernyh Zonnyh Sistem* (Fizmatlit, Moscow, 2012).

[32] The DMFT spectral densities were calculated as $-\mathrm{Im}G_R(\omega)/\pi$ with

$$G_R(\omega) = \int_{-\infty}^{\infty} dx \frac{A_0(x)}{\omega - x - \Sigma_R(\omega)}$$

after analytical continuation of the self-energy. This allows for resolving features like sharp peaks in the spectral density that would be smeared out by direct analytic continuation of the local Green's function in Matsubara frequencies.

[33] Y. M. Vilk and A.-M. S. Tremblay, J. Phys. I (France) **7**, 1309 (1997).

[34] M. R. Norman, H. Ding, M. Randeria, J. C. Campuzano, T. Yokoya, T. Takeuchi, T. Takahashi, T. Mochiku, K. Kadowaki, P. Guptasarma, and D. G. Hinks, Nature (London) **392**, 157 (1998).

[35] T. Timusk and B. Statt, Rep. Prog. Phys. **62**, 61 (1999).

[36] B. Keimer, S. A. Kivelson, M. R. Norman, S. Uchida, and J. Zaanen, Nature (London) **518**, 179 (2015).

[37] P. A. Lee, N. Nagaosa, and X.-G. Wen, Rev. Mod. Phys. **78**, 17 (2006).

[38] G. Sordi, P. Sémon, K. Haule, and A.-M. S. Tremblay, Phys. Rev. Lett. **108**, 216401 (2012).

[39] O. Gunnarsson, T. Schäfer, J. P. F. LeBlanc, E. Gull, J. Merino, G. Sangiovanni, G. Rohringer, and A. Toschi, Phys. Rev. Lett. **114**, 236402 (2015).

[40] W. Wu, M. S. Scheurer, S. Chatterjee, S. Sachdev, A. Georges, and M. Ferrero, Phys. Rev. X **8**, 021048 (2018).

[41] M. V. Sadovskii, I. A. Nekrasov, E. Z. Kuchinskii, T. Pruschke, and V. I. Anisimov, Phys. Rev. B **72**, 155105 (2005).

[42] Y. Z. Zhang and M. Imada, Phys. Rev. B **76**, 045108 (2007).

[43] A. A. Katanin, A. Toschi, and K. Held, Phys. Rev. B **80**, 075104 (2009).

[44] E. Gull, O. Parcollet, and A. J. Millis, Phys. Rev. Lett. **110**, 216405 (2013).

[45] T. Schäfer, F. Geles, D. Rost, G. Rohringer, E. Arrigoni, K. Held, N. Blümer, M. Aichhorn, and A. Toschi, Phys. Rev. B **91**, 125109 (2015).

[46] G. Rohringer, H. Hafermann, A. Toschi, A. A. Katanin, A. E. Antipov, M. I. Katsnelson, A. I. Lichtenstein, A. N. Rubtsov, and K. Held, Rev. Mod. Phys. **90**, 025003 (2018).

[47] D. Rohe and C. Honerkamp, SciPost Phys. **9**, 84 (2020).

[48] T. Schäfer, N. Wentzell, F. Šimkovic IV, Y.-Y. He, C. Hille, M. Klett, C. J. Eckhardt, B. Arzhang, V. Harkov, F.-M. Le Régent, A. Kirsch, Y. Wang, A. J. Kim, E. Kozik, E. A. Stepanov, A. Kauch, S. Andergassen, P. Hansmann, D. Rohe, Y. M. Vilk *et al.*, Phys. Rev. X **11**, 011058 (2021).

[49] F. Gebhard, *The Mott Metal-Insulator Transition* (Springer, Berlin, 1997).

[50] The calculation of scattering in this paper is still possible within equilibrium DMFT theory; whereas the nonequilibrium processes of [15] required the nonequilibrium DMFT [77,78].

[51] As we do not have a linear quasiparticle renormalization in the self-energy, we plot $1/\tau(\omega) = 2\mathrm{Im}\Sigma(\omega)$; $Z = 1$ in Eq. (10).

[52] S.-K. Mo, H.-D. Kim, J. W. Allen, G.-H. Gweon, J. D. Denlinger, J.-H. Park, A. Sekiyama, A. Yamasaki, S. Suga, P. Metcalf, and K. Held, Phys. Rev. Lett. **93**, 076404 (2004).

[53] M. Karski, C. Raas, and G. S. Uhrig, Phys. Rev. B **77**, 075116 (2008).

[54] M. Ganahl, M. Aichhorn, H. G. Evertz, P. Thunström, K. Held, and F. Verstraete, Phys. Rev. B **92**, 155132 (2015).

[55] S.-S. B. Lee, J. von Delft, and A. Weichselbaum, Phys. Rev. Lett. **119**, 236402 (2017).

[56] M. Granath and J. Schött, Phys. Rev. B **90**, 235129 (2014).

[57] S. Nishimoto, F. Gebhard, and E. Jeckelmann, J. Phys.: Condens. Matter **16**, 7063 (2004).

[58] E. Kalinowski and F. Gebhard, J. Low Temp. Phys. **126**, 979 (2002).

[59] J. Hubbard, Proc R. Soc. London **281**, 401 (1964).

[60] P. G. J. van Dongen and C. Leinung, Ann. Phys. **509**, 45 (1997).

[61] J. K. Freericks and V. Zlatić, Rev. Mod. Phys. **75**, 1333 (2003).

[62] M. E. Sorantin, A. Dorda, K. Held, and E. Arrigoni, Phys. Rev. B **97**, 115113 (2018).

[63] J. Kanamori, Prog. Theor. Phys. **30**, 275 (1963).

[64] J. C. Slater, *Quantum Theory of Atomic Structure* (McGraw-Hill, New York, 1960).

[65] J. S. Griffith, *The Theory of Transition-MetalIons* (Cambridge University Press, Cambridge, 1971).

[66] T. Ribic, E. Assmann, A. Tóth, and K. Held, Phys. Rev. B **90**, 165105 (2014).

[67] J. Bünemann and F. Gebhard, J. Phys.: Condens. Matter **29**, 165601 (2017).

[68] F. Maislinger and H. G. Evertz, arXiv:2007.16201.
[69] A. Kauch, P. Worm, P. Prauhart, M. Innerberger, C. Watzenböck, and K. Held, Phys. Rev. B **102**, 245125 (2020).
[70] E. Manousakis, Phys. Rev. B **82**, 125109 (2010).
[71] E. Assmann, P. Blaha, R. Laskowski, K. Held, S. Okamoto, and G. Sangiovanni, Phys. Rev. Lett. **110**, 078701 (2013).
[72] D. C. Montgomery and G. C. Runger, *Applied Statistics and Probability for Engineers*, 7th ed. (Wiley, New York, 2018).
[73] H. Kajueter, Ph.D. thesis, Rutgers University, 1996.
[74] H. Kajueter and G. Kotliar, Phys. Rev. Lett. **77**, 131 (1996).
[75] M. Potthoff, T. Wegner, and W. Nolting, Phys. Rev. B **55**, 16132 (1997).
[76] A. Georges and W. Krauth, Phys. Rev. Lett. **69**, 1240 (1992).
[77] J. K. Freericks, V. M. Turkowski, and V. Zlatić, Phys. Rev. Lett. **97**, 266408 (2006).
[78] H. Aoki, N. Tsuji, M. Eckstein, M. Kollar, T. Oka, and P. Werner, Rev. Mod. Phys. **86**, 779 (2014).